ACS APPLIED MATERIALS & INTERFACES

Research Article

www.acsami.org

PDMS-based Triboelectric and Transparent Nanogenerators with ZnO Nanorod Arrays

Yeong Hwan Ko, Goli Nagaraju, Soo Hyun Lee, and Jae Su Yu*

Department of Electronics and Radio Engineering, Institute for Laser Engineering, Kyung Hee University, 1 Seocheon-dong, Giheung-gu, Yongin-si, Gyeonggi-do 446-701, Republic of Korea

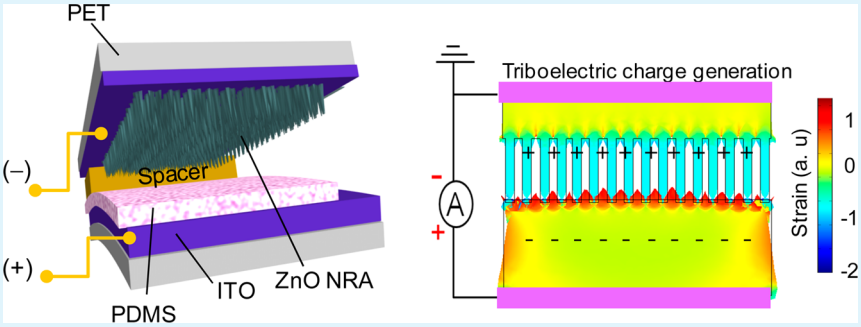

ABSTRACT: Vertically-grown ZnO nanorod arrays (NRAs) on indium tin oxide (ITO)-coated polyethylene terephthalate (PET), as a top electrode of nanogenerators, were investigated for the antireflective property as well as an efficient contact surface in bare polydimethysiloxane (PDMS)-based triboelectric nanogenerators. Compared to conventional ITO-coated PET (i.e., ITO/PET), the ZnO NRAs considerably suppressed the reflectance from 20 to 9.7% at wavelengths of 300−1100 nm, creating a highly transparent top electrode, as demonstrated by theoretical analysis. Also, the interval time between the peaks of generated output voltage under external pushing forces was significantly decreased from 1.84 to 0.19 s because the reduced contact area of the PDMS by discrete surfaces of the ZnO NRAs on ITO/PET causes a rapid sequence for triboelectric charge generation process including rubbing and separating. Therefore, the use of this top electrode enabled to operate the transparent PDMS-based triboelectric nanogenerator at high frequency of external pushing force. Under different external forces of 0.3−10 kgf, the output voltage and current were also characterized.

KEYWORDS: *ZnO nanorod arrays, triboelectric nanogenerators, antireflection, PDMS*

1. INTRODUCTION

In recent years, nanogenerators including piezotronics, piezoelectrics and triboelectrics have been considered as a promising alternative for energy harvesting and renewable resources in green nanotechnology.[1−3] Owing to flexible, durable, and light weight properties, in advances, they can be available for the mobile, portable and wearable electronic devices supported by self-power generation.[4−6] Among the various kinds of nanogenerators, the triboelectric nanogenerator has attracted much attention because of its high energy conversion efficiency, scalability, and simplicity for fabrication.[7,8] Accordingly, triboelectric nanogenerators based on polymer materials, such as polydimethysiloxane (PDMS) and Kapton, have been developed for an enhancement of output power and conversion efficiency by using micro- or nano-patterned surfaces.[9,10] Positive and negative charges are distributed according to the triboelectric tendency when both the surfaces contact and rub against each other by external mechanic force, and the flow of electric charges is created by separating and neutralization processes.[11,12] Thus, the surface morphology and interface between the polymer material and electrode are very important for the triboelectric charge generation.

However, there still remain some difficulties including the needs of a soft imprint technique for its fabrication. To fabricate such samples, the master molds with inverted patterns should be prepared by lithography and etching processes. Additionally, the patterned PDMS should be carefully separated from the master molds under limited sizes. If bare PDMS is directly utilized for triboelectric nanogenerators, it would provide essential advantages in manufacturing the nanogenerators and be a promising solution for cost-effective mass production. For instance, the large scale of bare PDMS is readily fabricated by simply preparing and curing the mixture of PDMS. This bare PDMS intends to be laminated on various electrically-conductive materials including ITO/PET, Al, and Cu foils owing to van der Waals forces, thus leading to a self-contacted PDMS with flexible electrode. However, such attachment causes drawbacks in the operation of triboelectric nanogenerators with conventional top electrode. Once the top electrode is contacted and rubbed with bare PDMS under

Received: January 14, 2014
Accepted: April 23, 2014
Published: April 23, 2014

   dx.doi.org/10.1021/am5018072 | ACS Appl. Mater. Interfaces 2014, 6, 6631−6637

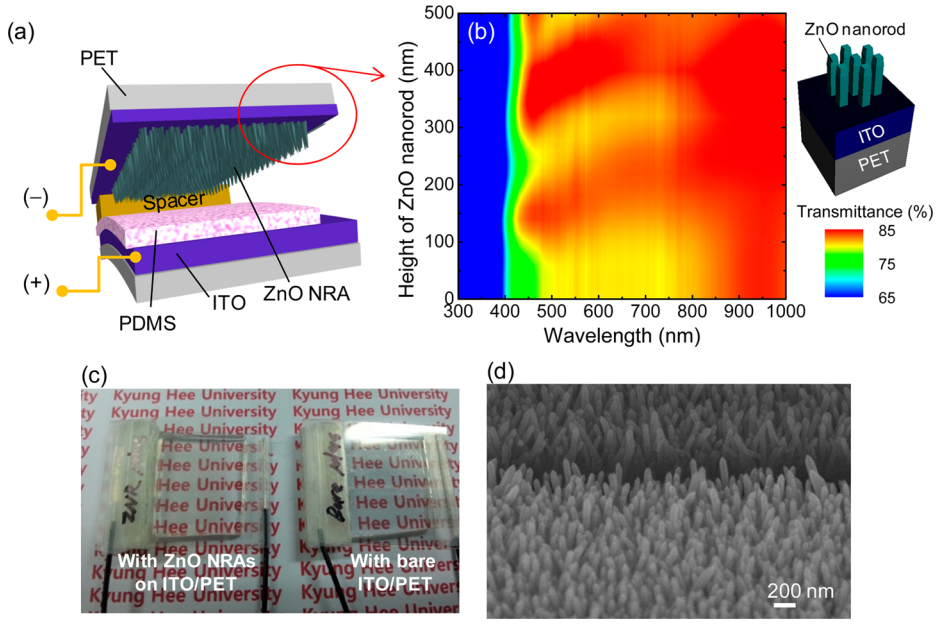

Figure 1. (a) Schematic diagram of the PDMS-based triboelectric nanogenerator with vertically-aligned ZnO NRAs on ITO/PET as a top electrode, (b) contour plot of calculated transmittances for different heights of ZnO nanorods and corresponding 3D modeling of ZnO NRAs, (c) photographical image of the two PDMS-based triboelectric nanogenerators with (left) and without (right) vertically-aligned ZnO NRAs, and (d) oblique-view FE-SEM image of the ZnO NRAs on ITO/PET.

external compression, it is difficult to be rapidly separated and to repeat the next cycle.

On the other hand, the fabrication technology for growing vertically-aligned ZnO nanorod arrays (NRAs) on various substrates, such as semiconductors, glasses, plastics and celluloses, by a facile chemical synthesis has been progressed for optoelectronic, photovoltaic, and piezoelectric applications.[13−15] Particularly, vertically-aligned ZnO NRAs on the transparent conductive oxide substrate such as aluminum doped ZnO or indium tin oxide (ITO) can be used as a highly transparent electrode for specific devices due to their antireflective characteristics.[16,17] Indeed, based on the effective medium theory, an antireflection structure is formed from the fact that the ZnO NRAs offered a graded effective refractive index profile for incident light with longer wavelength than their size.[18] In addition, discrete surfaces of ZnO NRAs would be desirable for triboelectric nanogenerators which require an efficient contact and interface to the surface of triboelectric polymer materials.

In this work, we fabricated transparent and triboelectric nanogenerators based on PDMS using vertically-aligned ZnO NRAs synthesized on the ITO-coated polyethylene terephthalate (PET) flexible substrate by an electrochemical deposition (ED) method as a top electrode. To evaluate the transparency of the prepared samples, the transmittance spectra were measured experimentally and analyzed theoretically. The effects of ZnO NRAs on the triboelectric charge generation property were also investigated under different external pushing forces and frequencies.

2. EXPERIMENTAL DETAILS

2.1. Fabrication of Samples. To obtain the vertically-aligned ZnO NRAs on ITO-coated PET (i.e., ITO/PET) substrate, the ED method was utilized by using a simple two-electrode system. Here, the platinum mesh and working sample act as an anode and cathode, repectively.[19] Prior to the synthesis of ZnO NRAs, the 2 × 2.5 cm^2 of ITO (200 nm)/PET (137 μm) substrate was cut and cleaned with acetone, methanol, and de-ionized (DI) water under ultrasonication. The ITO/PET (surface resistivity 60 Ω/sq) was purchased from Sigma-Aldrich Corporation. Then, the ZnO seed layer of 15 nm was deposited by performing the radio-frequency (RF) magnetron sputtering with a ZnO target of 99.999% purity. The deposition was carried out in an argon gas environment at 6 mTorr of process pressure and 100 W of RF power. Meanwhile, growth solution was prepared by mixing 10 mM zinc nitrate hexahydrate ($Zn(NO_3)_2 \cdot 6H_2O$) and 10 mM hexamethylenetetramine (HMT, $(CH_2)_6N_4$) in 900 mL of DI water, and the temperature was maintained at ∼78 °C. When the ZnO seed-coated ITO/PET was dipped into the growth solution, the external cathodic voltage of −2 V was applied between the two electrodes. During the ED process, the growth solution was kept to homogeneous mixture by stirring. After 1 h, the sample was carefully pulled out and rinsed by flowing DI water. On the other side, PDMS was prepared as a triboelectric material. After the base and curing agent of the PDMS was stirred vigorously with a weight ratio of 5:1, the mixture was degassed in a vacuum chamber. Then, it was poured into a flat Petri dish until the thickness became 1.5 mm and cured in oven at 75 °C for 1 h. To fabricate triboelectric nanogenerators, the 2 × 2 cm of PDMS was laminated on the ITO/PET substrate.

2.2. Characterization and Measurement of Samples. The morphology and crystallinity of ZnO NRAs on ITO/PET were observed by employing a field-emission scanning electron microscope (FE-SEM; LEO SUPRA 55, Carl Zeiss), a transmission electron microscope (TEM; JEM 200CX, JEOL), and an X-ray diffraction (XRD; Mac Science, M18XHF-SRA). For optical transmittance measurements, an UV-vis-NIR spectrophotometer (Cary 5000, Varian) was used. For theoretical analysis, a rigorous coupled-wave analysis (RCWA) simulation was carried out using a commercial software (DiffractMOD 3.1, Rsoft Design Group). In order to measure output voltage and current characteristics of triboelectric nanogenerators by applying external mechanical forces, a programmable multimeter/picoammeter (Keithley 2000/6487) and an indicator (BONGSHIN, Inc.) were used. The external pushing of 0.3-10 kgf was applied to the top surface of triboelectric nanogenerators by gently touching the load cell with human fingers so that the selected range of pushing force was adjusted using an indicator for monitoring.[20] For

dx.doi.org/10.1021/am5018072 | ACS Appl. Mater. Interfaces 2014, 6, 6631−6637

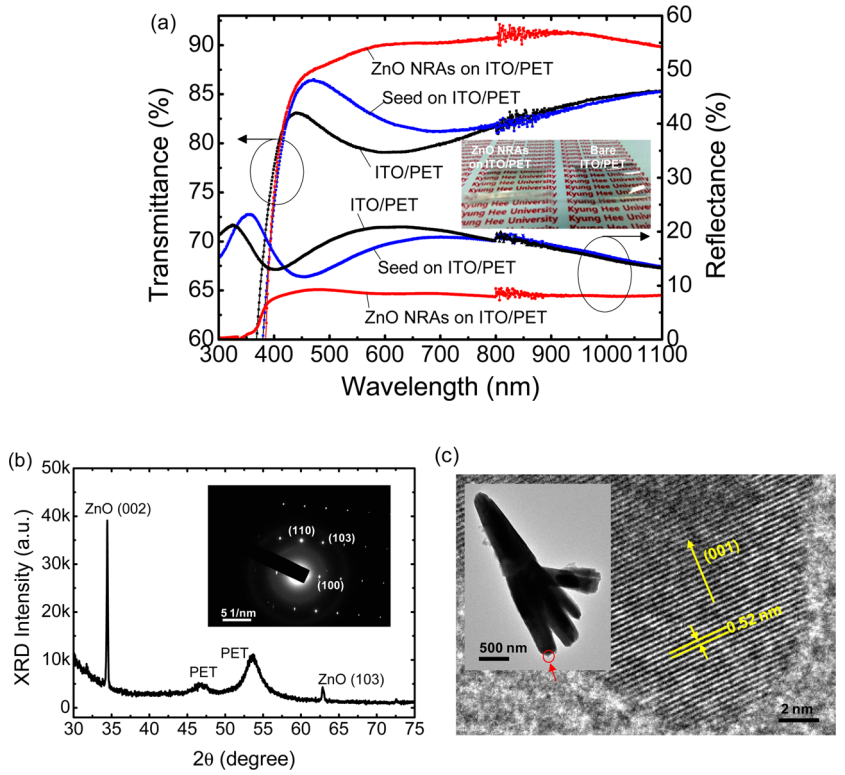

Figure 2. (a) Measured transmittance and reflectance spectra of the ITO/PET, the ZnO seed-coated ITO/PET, and the ZnO NRAs on ITO/PET, (b) HRTEM image of ZnO nanorod and (c) 2θ scan XRD patterns of the ZnO NRAs on ITO/PET. The insets of a and c show the photographic image of the bare ITO/PET and the ZnO NRAs on ITO/PET, and the SAED pattern, respectively.

the synchronization with specific frequency of pushing, the metronome was utilized during the operation.

3. RESULTS AND DISCUSSION

Figure 1a shows the schematic diagram of the PDMS-based triboelectric nanogenerator with vertically-aligned ZnO NRAs on ITO/PET as a top electrode. The fabricated triboelectric nanogenerators consisted of top and bottom electrodes. The vertically-aligned ZnO NRAs were formed on the top ITO/PET and the PDMS was laminated on the bottom ITO/PET. For generating electric charges by pushing and separating processes, the electrodes were set apart from each other by inserting the spacer and the conductive wires were contacted, as shown in Figure 1a. In order to estimate the transparency properties of vertically-aligned ZnO NRAs on ITO/PET, the transmittance was calculated via the RCWA simulation which could accurately predict the transmittance of nanostructures by solving the Maxwell's equation with spatial harmonics.[21] After the diffracted electromagnetic waves are determined by satisfying the boundary conditions at the interface of specific region, the optical transmission efficiency can be obtained from the transmitted diffraction elements. Figure 1b shows the contour plot of calculated transmittances as a function of the height of ZnO nanorods and the corresponding three-dimensional (3D) modeling of ZnO NRAs. The thicknesses of ITO/PET were approximately 200 nm/127 μm and the ZnO nanorods were aligned with widths of ~45 nm and heights of ~360 nm from the FE-SEM images. The ITO/PET without ZnO NRAs (i.e., the height of ZnO nanorods is zero) exhibited low transmittances of <81% over a wavelength range of 430-750 nm. For the ZnO seed-coated ITO/PET, the transmittance was slightly increased as compared to bare ITO/PET. This would be caused by the fact that the deposited ZnO thin film (15 nm) decreases the difference of refractive index between air and the ITO, which reduces the Fresnel reflections. As the height of ZnO nanorods was increased, the transmittance was gradually increased. Indeed, this increase of transmittance is due to the effective refractive index (n_{eff}) of ZnO NRAs which relaxes the difference of refractive index between air and the ITO/PET substrate, thus leading to an antireflection property.[17] Based on the effective medium theory, the n_{eff} can be obtained by $n_{eff} = [f_{ZnO}n_{ZnO}^{2/3} + f_{air}n_{air}^{2/3}]^{3/2}$, where n_{ZnO}/n_{air} and f_{ZnO}/f_{air} are the refractive index and volume fraction of ZnO/air, respectively. When the height of ZnO nanorods was increased, somewhat fluctuations of transmittance were caused by a fact that the ZnO NRAs serve as an interference layer with an effectively graded refractive index profile. For heights above 350 nm, high transmittances of >85% were observed over a wide range of wavelengths. As can be seen in Figure 1c, the photographical images of the two PDMS-based triboelectric nanogenerators with (left) and without (right) vertically-aligned ZnO NRAs confirmed that the top electrode of ZnO NRAs on ITO/PET made the triboelectric nanogenerator more transparent. To obtain the FE-SEM images, the grown ZnO NRAs on ITO/PET substrate were strongly folded for several times and then the part of cracks was zoomed in, as shown in Figure 1d. At an external applied voltage of -2 V for 1 h, the size and height of ZnO nanorods were approximately 30-80 nm and 340-400 nm, respectively.

Figure 2a shows the measured transmittance and reflectance spectra of the ITO/PET, the ZnO seed-coated ITO/PET, and the ZnO NRAs on ITO/PET. As compared with the bare ITO/PET, the seed-coated ITO/PET also exhibited a slightly increased transmittance spectrum. For the ZnO NRAs on ITO/

dx.doi.org/10.1021/am5018072 | ACS Appl. Mater. Interfaces 2014, 6, 6631−6637

PET, it is clearly observed that the transmittance was considerably increased at wavelengths of 400-1100 nm. In the wavelength range of 600−1100 nm, high transmittances of >90% were achieved. As previously explained, the high transparency was mainly due to the antireflection property of vertically-aligned ZnO NRAs, which was also confirmed by measured reflectance spectra. When compared with the ITO/PET and the ZnO NRA on ITO/PET, the ZnO NRAs largely reduced the reflectance in the overall range of wavelengths. Especially, the reflectance was decreased from 21.3 to 8.1% at the wavelength of 600 nm. As shown in the inset of Figure 2a, it can be observed that the ZnO NRAs on ITO/PET are flexible with a high transparent property. Under 375 nm of wavelength, the reflectance was dramatically reduced and it reached to zero with further decreasing the wavelength. This is closely related with a direct bandgap of ZnO ($\lambda \sim 375$ nm). Thus, most of photons were absorbed when the energy of incident light was larger than the bandgap energy of the ZnO. From the XRD patterns of ZnO NRAs on ITO/PET, as shown in Figure 2b, the dominant XRD peak of ZnO (002) appeared at 34.44°. The two broad XRD peaks of PET were also observed at 46.83 and 53.74°. The strong and sharp XRD peak of ZnO (002) indicated that the ZnO nanorod was perpendicularly grown on the seed layer and well crystallized along the c-axis of the hexagonal wurzite structure. In the inset of Figure 2b, the selected area electron diffraction (SAED) pattern of a ZnO nanorod was clearly observed, confirming the single-crystal wurtzite structure. Figure 2c shows the high-resolution TEM (HRTEM) image for the selected area of a ZnO nanorod (highlighted by a red circle in the TEM image). From the HRTEM observation, the lattice fringe with a d-spacing of 0.52 nm was in good agreement with the lattice constant (001) plane of ZnO structure.

Figure 3a represents the pushing test procedure of samples: (i) monitoring the external pushing force, (ii) pushing and (iii) separating between the top and bottom electrodes (i.e., the ZnO NRAs on ITO/PET and the PDMS-laminated ITO/PET). By using a load cell, the different pushing forces from 0.3 to 10 kgf were applied and estimated on the nanogenerator. Figure 3b,c shows the measured output voltages of the PDMS-based triboelectric nanogenerators using the ITO/PET top electrode without and with vertically-aligned ZnO NRAs under the external pushing force of 0.3 kgf and the frequency of 0.25 Hz. Here, the top electrode was connected to a ground (i.e., earth) for consistent measurement. Two voltage curves displayed the repeated positive and negative peaks at the moments of pushing and separating, respectively. This directionality of the peaks was related to the triboelectric tendency and electric charge flowing, as is discussed in detail in Figure 4. To estimate the switching speed of triboelectric nanogenerators by applying the external pushing force, the internal time was defined as a consuming time between the positive and next negative peaks. For the top electrode without ZnO NRAs, the long interval time was measured to be 1.84 s. In fact, the PDMS tends to be adhesive to various solid surfaces owing to their van der Waals forces.[22] When the top electrode was contacted to the surface of PDMS, it was laminated spontaneously and then prolonged adhesion. In contrast, the use of ZnO NRAs significantly reduced the internal time to 0.19 s, which enables us to operate the nanogenerator at the higher frequency of external pushing. This short interval time was caused by the discrete surface and rigidness of ZnO NRAs. After the PDMS was compressed and deformed by ZnO NRAs,

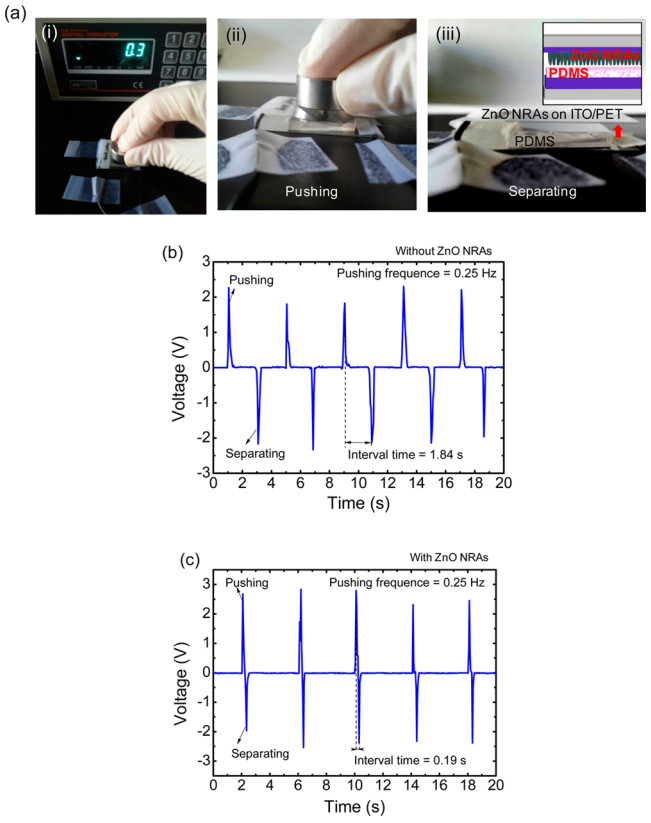

Figure 3. (a) Photographic images for (i) monitoring the external pushing force on the PDMS-based triboelectric nanogenerator, (ii) pushing and (iii) separating between the top and bottom electrodes (i.e., the ZnO NRAs on ITO/PET and the PDMS-laminated ITO/PET), and measured output voltages of the PDMS-based triboelectric nanogenerators using the ITO/PET top electrode (b) without and (c) with vertically-aligned ZnO NRAs under the external pushing force of 0.3 kgf and the frequency of 0.25 Hz.

it was recovered with minimizing the contact area between both surfaces, as shown in the inset of Figure 3aiii.

Figure 4a shows the schematic diagram for operating mechanism of the PDMS-based triboelectric nanogenerator with vertically-aligned ZnO NRAs on ITO/PET as a top electrode. Here, the calculated strain distribution from the simulation is also shown. It could be assumed that the measured output voltage/current is attributed mainly to the triboelectric charge generation because the piezoelectric charges would be rarely generated when the ZnO NRAs are bent and contacted to bare PDMS. For the ZnO NRAs on ITO/PET with gold (Au)-coated PET as a typical piezoelectric nanogenerator,[23] we observed the relatively very low charge generation with average output current of ∼3.6 nA. For this, the strain distribution of the PDMS-based triboelectric nanogenerator and ZnO NRAs was theoretically calculated using a commercial software (COMSOL 3.2, stress−strain application mode) for investigating the contact property under compression. In the practical numerical calculation, the size and height of ZnO nanorods were determined to 50 and 360 nm, respectively, from the FE-SEM images. Considering the density and elastic constant of each material, the Navier's equation (i.e., $-\nabla\cdot\sigma = F$. σ, stress tensor; F, volume force) was solved by utilizing the finite element method. Herein, the 0.3 kgf/cm^2 was assumed as a pushing force. When the ZnO NRAs are compressed and contacted with PDMS, the mechanical energy

dx.doi.org/10.1021/am5018072 | ACS Appl. Mater. Interfaces 2014, 6, 6631−6637

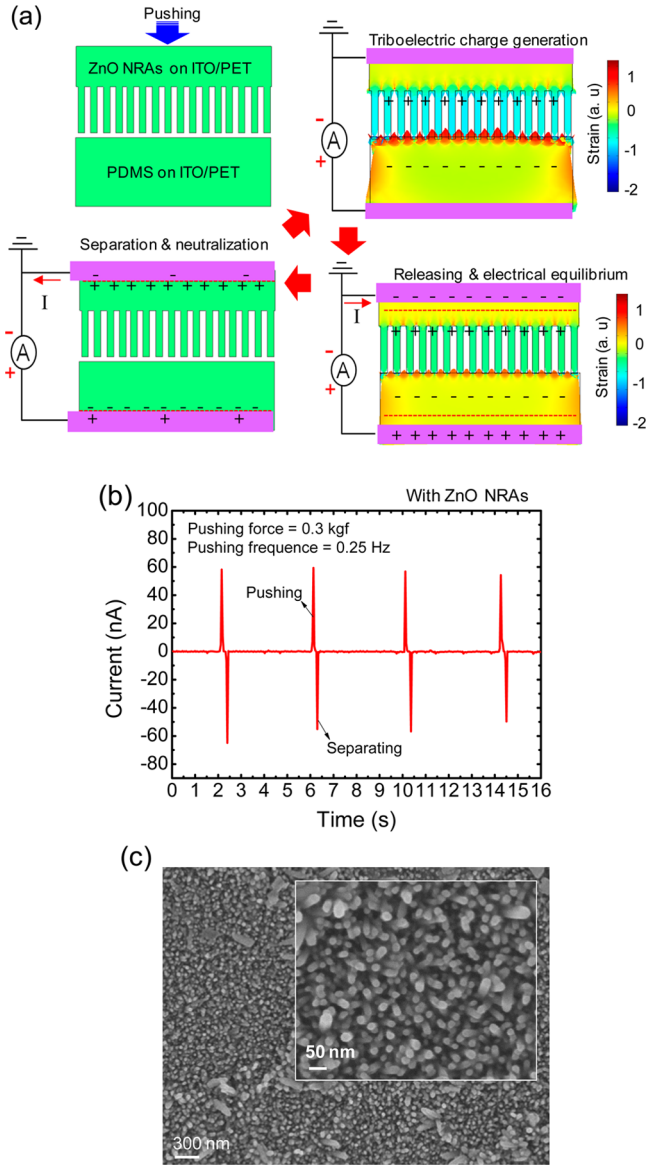

Figure 4. (a) Schematic diagram for operating mechanism and strain distribution of the PDMS-based triboelectric nanogenerator using the top electrode with vertically-aligned ZnO NRAs from the simulation, (b) measured output current of the corresponding sample, and (c) FE-SEM image of the top electrode of ZnO NRs after repetitive mechanical experiments.

is transformed from the nanorods to the surface of PDMS and a deformation occurs. The ZnO NRAs were dominantly stressed in normal direction and they strictly pressed the surface of PDMS. While the PDMS was released after pushing, the contact surface was partially distributed at the top of ZnO nanorods. Therefore, it could be expected that the ZnO NRAs provide an efficient separation from the PDMS. According to the triboelectric tendency,[11] as shown in Figure 4a, the negative and positive charges were distributed at the PDMS and top electrode, respectively, after rubbing and contacting against each other. As a result, the electric field was induced between both regions, which creates a flow of electric charges. During the releasing and tending toward an electrical equilibrium, the electrons flow continuously from the top electrode to the bottom electrode. Then, the direction was reversed after the separation because the electric charges were moved for neutralization. As shown in the measured output current of the corresponding sample of Figure 4b, the positive/negative peaks were repeated at pushing/separating points, which well agreed with the current flow, as depicted in the schematic diagram. Under 0.3 kgf/0.25 Hz of pushing force/frequency, the averaged output current was obtained as 58.7 nA. To clarify the adhesion property of ZnO NRAs on the ITO/PET, the FE-SEM images of the surface of ZnO NRAs of the tested samples for repetitive mechanical experiments are shown in Figure 4c. Somewhat broken ZnO nanorods were sparsely detached on the surface, which was obtained from the top electrode of ZnO NRAs during the pushing test. From the magnified view of the FE-SEM image in the inset, it is evident that the grown ZnO nanorods are durable to sustain the adhesion and alignment on the ITO/PET. After repetition of mechanical compression with pushing forces of 1.2−10 kgf, most of ZnO NRAs remained intact.

Figure 5 shows the (a) pushing frequency and (b) external pushing force dependent output (i) voltage and (ii) current characteristics of the PDMS-based triboelectric nanogenerator with vertically-aligned ZnO NRAs on ITO/PET. To investigate the effect of pushing frequency, it was varied from 0.5 to 4 Hz under the external force of 0.3 kgf. It is evident that the output voltage and current were gradually increased as the pushing frequency was increased. At each frequency, the averaged voltage/current values were obtained as 2.13 V/67.3 nA (0.5 Hz), 2.43 V/73.6 nA (1 Hz), 2.74 V/86.1 nA (2 Hz), and 3.62 V/112.7 nA (4 Hz). This performance improvement is attributed to the accumulated residual charges were accumulated by an imperfection of neutralization due to rapid external pushing cycles, resulting in the increase of triboelectric potential.[24] In Figure 5b, the output voltage and current could be also increased with increasing the external pushing force. Under 1 Hz of pushing frequency, the averaged voltage/current was increased from 3.31 V/83.4 nA to 5.34 V/181.4 nA. This can be explained by the fact that more friction and deformation of PDMS under higher external mechanical force increases the amount of generated triboelectric charges. As compared to previous reports on the efficient fabrication method of triboelectric nanogenerators,[24] these results are comparable and encouraging in the research of PDMS-based triboelectric nanogenerators. To examine a reliability of the sample, the output voltage and current were measured under external pushing forces with repetitions of 1200 times, as shown in Figure 5c. Under 3.5−4 kgf of pushing force and 0.25 Hz of frequency, the PDMS-based triboelectric nanogenerators with ZnO NRAs exhibited regular output voltage and current characteristics for numerous mechanical pushing operations. As the operation time was increased to 3000 s, the peak values of output voltage and current could be still retained, which supported that the top electrode of ZnO NRAs was maintainable to generate triboelectric charges for long-term operation.

4. CONCLUSIONS

In summary, the vertically-aligned ZnO NRAs were synthesized on ITO/PET via the ED method and used for the top electrode of the PDMS-based triboelectric nanogenerators. The synthesized ZnO NRAs exhibited a good antireflection property and discrete surface morphology, which makes the triboelectric nanogenerator more favorable for higher transparency and faster operation. The top electrode with vertically-aligned ZnO NRAs on ITO/PET had high transmittances of >85% over a

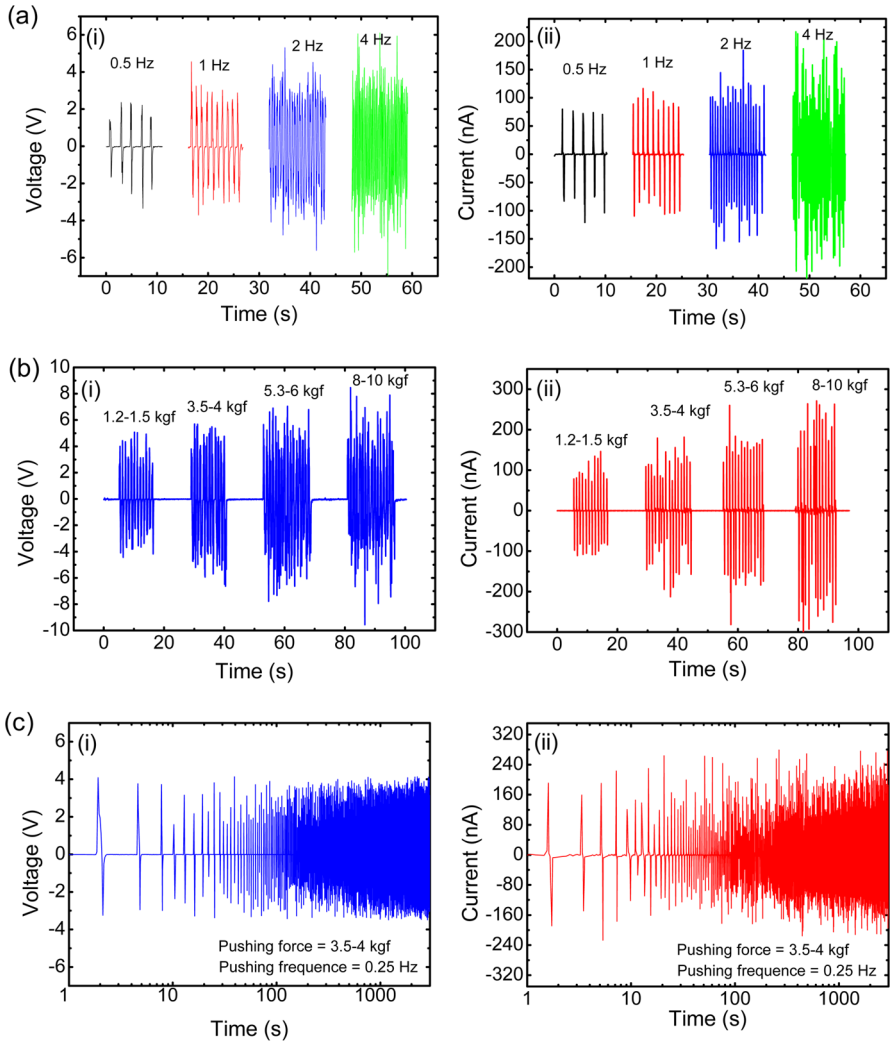

Figure 5. Measured output (i) voltage and (ii) current of the PDMS-based triboelectric nanogenerator with vertically-aligned ZnO NRAs on ITO/PET under different (a) external pushing frequencies (0.5−4 Hz) and (b) pushing forces (1.2−10 kgf). For testing the reliability, panel c also shows the measured output voltage and current of the same sample for 1200 repetitions of external pushing.

wide range of wavelengths and a short interval time of 0.19 s was obtained. Under high pushing frequency and force, the improved output voltage/current of 3.62 V/112.7 nA (4 Hz under 0.3 kgf) and 5.34 V/181.4 nA (1 Hz under 8−10 kgf) were achieved. These results suggest that the incorporation of vertically-aligned ZnO NRAs into the PDMS-based triboelectric nanogenerators can enhance their transparency and performance for various energy harvesting applications.

AUTHOR INFORMATION

Corresponding Author

*J. S. Yu. E-mail: jsyu@khu.ac.kr.

Notes

The authors declare no competing financial interest.

ACKNOWLEDGMENTS

This research was supported by Basic Science Research Program through the National Research Foundation of Korea (NRF) funded by the Ministry of Science, ICT and Future Planning (No. 2013-068407).

REFERENCES

(1) Yu, R.; Wu, W.; Ding, Y.; Wang, Z. L. GaN Nanobelt-Based Strain-Gated Piezotronic Logic Devices and Computation. *ACS Nano* **2013**, *7*, 6403−6409.

(2) Wang, Z. L.; Song, J. Piezoelectric Nanogenerators Based on Zinc Oxide Nanowire Arrays. *Science* **2006**, *312*, 242−246.

(3) Lin, Z. H.; Zhu, G.; Zhou, Y. S.; Yang, Y.; Bai, P.; Chen, J.; Wang, Z. L. A Self-Powered Triboelectric Nanosensor for Mercury Ion Detection. *Angew. Chem., Int. Ed.* **2013**, *52*, 1−6.

(4) Bai, P.; Zhu, G.; Lin, Z.-H.; Jing, Q.; Chen, J.; Zhang, G.; Ma, J.; Wang, Z. L. Integrated Multilayered Triboelectric Nanogenerator for Harvesting Biomechanical Energy from Human Motions. *ACS Nano* **2013**, *7*, 3713−3719.

(5) Meng, B.; Tang, W.; Too, Z.; Zhang, X.; Han, M.; Liu, W.; Zhang, H. A Transparent Single-Friction-Surface Triboelectric Generator and Self-Powered Touch Sensor. *Energy Environ. Sci.* **2013**, *6*, 3235−3240.

(6) Lee, M.; Chen, C. Y.; Wang, S.; Cha, S. N.; Park, Y. J.; Kim, J. M.; Chou, L. J.; Wang, Z. L. A Hybrid Piezoelectric Structure for Wearable Nanogenerators. *Adv. Mater.* **2012**, *24*, 1759−1764.

(7) Hou, T. C.; Yang, Y.; Zhang, H.; Chen, J.; Chen, L. J.; Wang, Z. L. Triboelectric Nanogenerator Built Inside Shoe Insole for Harvesting Walking Energy. *Nano Energy* **2013**, *2*, 856−862.

(8) Zhu, G.; Chen, J.; Liu, Y.; Bai, P.; Zhou, Y. S.; Jing, Q.; Pan, C.; Wang, Z. L. Linear-Grating Triboelectric Generator Based on Sliding Electrification. *Nano Lett.* **2013**, *13*, 2282−2289.
(9) Zhang, X. S.; Han, M. D.; Wang, R. X.; Zhu, F. Y.; Li, Z. H.; Wang, W.; Zhang, H. X. Frequency-Multiplication High-Output Triboelectric Nanogenerator for Sustainably Powering Biomedical Microsystems. *Nano Lett.* **2013**, *13*, 1168−1172.
(10) Zhu, G.; Pan, C.; Guo, W.; Chen, C. Y.; Zhou, Y.; Yu, R.; Wang, Z. L. Triboelectric-Generator-Driven Pulse Electrodeposition for Micropatterning. *Nano Lett.* **2012**, *12*, 4960−4965.
(11) Fan, F. R.; Lin, L.; Zhu, G.; Wu, W.; Zhang, R.; Wang, Z. L. Transparent Triboelectric Nanogenerators and Self-Powered Pressure Sensors Based on Micropatterned Plastic Films. *Nano Lett.* **2012**, *12*, 3109−3114.
(12) Zhu, G.; Lin, Z. H.; Jing, Q.; Bai, P.; Pan, C.; Yang, Y.; Zhou, Y.; Wang, Z. L. Toward Large-Scale Energy Harvesting by a Nanoparticle-Enhanced Triboelectric Nanogenerator. *Nano Lett.* **2013**, *13*, 847−853.
(13) Hatch, S. M.; Briscoe, J.; Dunn, S. A Self-Powered ZnO-Nanorod/CuSCN UV Photodetector Exhibiting Rapid Response. *Adv. Mater.* **2013**, *25*, 867−871.
(14) Liu, J.; Wu, W.; Bai, S.; Qin, Y. Synthesis of High Crystallinity ZnO Nanowire Array on Polymer Substrate and Flexible Fiber-Based Sensor. *ACS Appl. Mater. Interface* **2011**, *3*, 4197−4200.
(15) Ko, Y. H.; Lee, S. H.; Yu, J. S. Performance Enhanced Piezoelectric ZnO Nanogenerators with Highly Rough Au Electrode Surfaces on ZnO Submicrorod Arrays. *Appl. Phys. Lett.* **2013**, *103*, 022911.
(16) Ko, Y. H.; Yu, J. S. Urchin-Aggregation Inspired Closely-Packed Hierarchical ZnO Nanostructures for Efficient Light Scattering. *Opt. Express* **2011**, *19*, 25935−25943.
(17) Ko, Y. H.; Kim, M. S.; Yu, J. S. Controllable Electrochemical Synthesis of ZnO Nanorod Arrays on Flexible ITO/PET Substrate and Their Structural and Optical Properties. *Appl. Surf. Sci.* **2012**, *259*, 99−104.
(18) Lee, Y. J.; Ruby, D. S.; Peters, D. W.; McKenzie, B. B.; Hsu, J. W. P. ZnO Nanostructures as Efficient Antireflection Layers in Solar Cells. *Nano Lett.* **2008**, *8*, 1501−1505.
(19) Lee, H. K.; Kim, M. S.; Yu, J. S. Effect of AZO Seed Layer on Electrochemical Growth and Optical Properties of ZnO Nanorod Arrays on ITO Glass. *Nanotechnology* **2011**, *22*, 445602.
(20) Choi, M. Y.; Choi, D.; Jin, M. J.; Kim, I.; Kim, S. H.; Choi, J. Y.; Lee, S. Y.; Kim, J. M.; Kim, S. W. Mechanically Powered Transparent Flexible Charge-Generating Nanodevices with Piezoelectric ZnO Nanorods. *Adv. Mater.* **2009**, *21*, 2185−2189.
(21) Chiu, C. H.; Yu, P.; Kuo, H. C.; Chen, C. C.; Lu, T. C.; Wang, S. C.; Hsu, S. H.; Cheng, Y. J.; Chang, Y. C. Broadband and Omnidirectional Antireflection Employing Disordered GaN Nanopillars. *Opt. Express* **2008**, *16*, 8748−8754.
(22) Yu, J.; Chary, S.; Das, S.; Tamelier, J.; Turner, K. L.; Israelachvili, J. N. Friction and Adhesion of Gecko-Inspired PDMS Flaps on Rough Surfaces. *Langmuir* **2012**, *28*, 11527−11534.
(23) Yu, A.; Li, H.; Tang, H.; Liu, T.; Jiang, P.; Wang, Z. L. Vertically Integrated Nanogenerator based on ZnO Nanowire Arrays. *Phys. Status Solidi RRL* **2011**, *5*, 162−164.
(24) Fan, F. R.; Tian, Z. Q.; Wang, Z. L. Flexible Triboelectric Generator! *Nano Energy* **2012**, *1*, 328−334.